Core/Shell Nanoparticles

International Edition: DOI: 10.1002/anie.201504676
German Edition: DOI: 10.1002/ange.201504676

Precisely Size-Tunable Magnetic/Plasmonic Core/Shell Nanoparticles with Controlled Optical Properties

*Di Yang, Xinchang Pang, Yanjie He, Yiquan Wang, Genxiang Chen, Wenzhong Wang, and Zhiqun Lin**

Abstract: *Star-like amphiphilic triblock copolymers were rationally designed and synthesized by combining two sequential atom-transfer radical polymerization reactions with a click reaction. Subsequently, a family of uniform magnetic/plasmonic core/shell nanoparticles was crafted by capitalizing on these triblock copolymers as nanoreactors. The diameter of the magnetic core and the thickness of the plasmonic shell could be independently and accurately controlled by varying the molecular weights (i.e., the chain lengths) of the inner and intermediate blocks of the star-like triblock copolymers, respectively. The surface plasmonic absorption of core/shell nanoparticles with different core diameters and shell thicknesses was systematically studied and theoretically modeled. This robust strategy provides easy access to a large variety of multifunctional nanoparticles with large lattice mismatches for use in optics, optoelectronics, catalysis, or bioimaging.*

Recent research has witnessed rapid advances in nanomaterial synthesis, which has led to the creation of a large variety of nanoparticles with well-controlled particle sizes and shapes.[1] As an important class of nanomaterials, core/shell nanoparticles that integrate two dissimilar materials with distinct functionalities have garnered considerable attention as they enable the synergistic coupling of the two constituents and thus offer opportunities for exploring the intriguing properties of their interface.[2] To effectively produce high-quality core/shell nanoparticles, a moderate lattice mismatch between the two different materials is often required (i.e., for epitaxial growth).[3] Notably, such conditioned material combinations significantly limit the core and shell material choice. Clearly, it is of great interest to develop alternative means of forming core/shell nanoparticles with a large lattice mismatch. Moreover, it is highly desirable to be capable of precisely tailoring the diameter of the core and the thickness of the shell as well as the surface properties of the core/shell nanoparticles. This, however, has yet to be explored in detail.

Among various core/shell nanoparticles, magnetic/noble metal hybrid nanoparticles have been widely studied as they possess intriguing magnetic/plasmonic and magnetic/catalytic properties, and they can be used in optical devices and chemical reactions as magnetically recyclable catalysts,[4] as well as in bioimaging, targeted drug delivery, and in vivo diagnosis.[5] In the latter context, magnetic Fe_3O_4 nanoparticles are the subject of extensive research for a myriad of biomedical applications, including controlled drug delivery, cancer therapy, and hyperthermia, owing to their low toxicity, good biocompatibility, and sensitivity to magnetic fields.[6] To improve the chemical stability of Fe_3O_4 nanoparticles by protecting them from corrosion and oxidation, it is advantageous to deposit a thin Au shell on the surface of the Fe_3O_4 core, leading to magnetic/plasmonic bifunctional core/shell nanoparticles for nonlinear photonic, sensing, and detection applications.[7] The Au shell exhibits intriguing optical properties, such as localized surface plasmon resonance and surface-enhanced Raman scattering.[8] To date, several synthetic routes to Fe_3O_4/Au core/shell (or vice versa) nanoparticles have been developed, including the reduction of a Au precursor in the presence of Fe_3O_4 nanoparticle seeds,[9,10] layer-by-layer assembly,[11] and the physisorption of small Au nuclei on Fe_3O_4 particles followed by subsequent electrodeless deposition.[12] However, Fe_3O_4 is an inverse spinel with a lattice parameter of 0.80903 nm (JCPDS No. 26-1136), and Au has a face-centered cubic structure with a lattice parameter of 0.40786 nm (JCPDS No. 04-0784).[13] Owing to the large lattice mismatch between Au and Fe_3O_4, it remains a grand challenge to prepare high-quality Fe_3O_4/Au core/shell nanoparticles with precisely controllable core diameters and shell thicknesses.

Herein, we report a viable strategy for crafting a series of uniform magnetic/plasmonic Fe_3O_4/Au core/shell nanoparticles with precisely controlled core diameters and shell thicknesses where the core and shell materials can be grown independently, virtually eliminating the restriction of lattice mismatch requirements, by capitalizing on amphiphilic nonlinear block copolymers as nanoreactors.

As illustrated in Scheme 1, a set of amphiphilic star-like poly(4-vinylpyridine)-*block*-poly(*tert*-butyl acrylate)-*block*-poly(ethylene oxide) (P4VP-*b*-P*t*BA-*b*-PEO) triblock copolymers with narrow molecular weight distributions for each block were rationally designed and synthesized by combining sequential atom transfer radical polymerization (ATRP) reactions of 4-vinylpyridine (4VP) and *tert*-butyl acrylate (*t*BA) [to form poly(4-vinylpyridine)-*block*-poly(*tert*-butyl acrylate) (P4VP-*b*-P*t*BA) based on β-cyclodextrin (β-CD)] with a click reaction (between azide-functionalized P4VP-*b*-P*t*BA with alkyne-terminated mPEO; Scheme 1a,b). The molecular weights (i.e., chain lengths) of the P4VP and P*t*BA

[*] X. Pang, Y. He, Prof. Z. Lin
School of Materials Science and Engineering
Georgia Institute of Technology
Atlanta, GA 30332 (USA)
E-mail: zhiqun.lin@mse.gatech.edu
Prof. D. Yang, Prof. Y. Wang, G. Chen, W. Wang
College of Science, Minzu University of China
Beijing 100081 (China)

Supporting information for this article is available on the WWW under http://dx.doi.org/10.1002/anie.201504676.

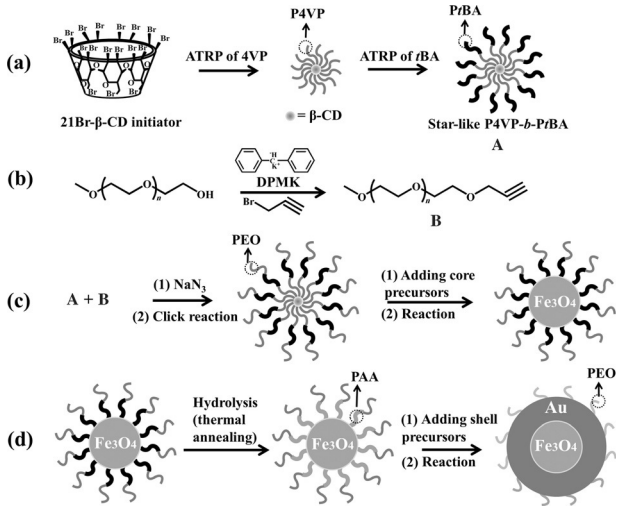

Scheme 1. Synthetic strategy for magnetic/plasmonic Fe_3O_4/Au core/shell nanoparticles based on star-like P4VP-*b*-P*t*BA-*b*-PEO triblock copolymers as nanoreactors. a) Synthesis of star-like P4VP-*b*-P*t*BA diblock copolymers employing a β-CD-based macroinitiator (21Br-β-CD). b) Synthesis of alkyne-terminated mPEO. c) Formation of magnetic Fe_3O_4 cores capped with P*t*BA-*b*-PEO (Fe_3O_4-P*t*BA-*b*-PEO). d) Formation of water-soluble PEO-capped Fe_3O_4/Au core/shell nanoparticles.

blocks could be readily tailored during the ATRP of their respective monomers (4VP and *t*BA). Subsequently, these amphiphilic star-like P4VP-*b*-P*t*BA-*b*-PEO triblock copolymers with P4VP and P*t*BA sections of various molecular weights were exploited as nanoreactors to create a family of magnetic/plasmonic Fe_3O_4/Au core/shell nanoparticles with precisely tunable Fe_3O_4 core diameters and Au shell thicknesses.

To craft core/shell nanoparticles, a mixed solvent system containing dimethylformamide (DMF) and diphenyl ether (DPE; DMF/DPE = 9:1, v/v) was used. DMF is a good solvent for all three blocks, whereas DPE is a poor solvent for the intermediate P*t*BA and outer PEO blocks but a good solvent for the inner P4VP blocks. Therefore, in the mixed DMF/DPE solvent system, the inner P4VP blocks retained their coil-like conformation, while the outer P*t*BA-*b*-PEO blocks collapsed, leading to the formation of a compact, yet spherical macromolecule, a unimolecular micelle. Consequently, the Fe_3O_4 precursors ($FeCl_2{\cdot}4H_2O$ and $FeCl_3{\cdot}6H_2O$) were preferentially encapsulated in the space occupied by star-like P4VP blocks owing to the hydrophilic nature of P4VP, and further transformed into Fe_3O_4 nanoparticles intimately connected by P*t*BA-*b*-PEO blocks (i.e., forming PEO-*b*-P*t*BA-functionalized Fe_3O_4 nanoparticles; Scheme 1c, right). This process is driven by the strong coordination interactions between the metal moieties of the Fe_3O_4 precursors (Fe^{2+} and Fe^{3+}) and the pyridyl groups in the P4VP blocks groups at the elevated temperature (see the Experimental Section in the Supporting Information).

Subsequently, the hydrophobic intermediate P*t*BA blocks were hydrolyzed into hydrophilic poly(acrylic acid) (PAA) blocks by thermally annealing PEO-*b*-P*t*BA-functionalized Fe_3O_4 nanoparticles in diphenyl ether at elevated temperature (see the Experimental Section in the Supporting Information), yielding PEO-*b*-PAA-functionalized Fe_3O_4 nanoparticles. Similar to the formation of Fe_3O_4 core nanoparticles described above, a DMF/DPE (9:1) mixed solvent system was also used to achieve the selective coordination interactions between the hydrophilic PAA blocks and the Au^{3+} ions in the Au precursor ($HAuCl_4$) within the area occupied by the PAA blocks (Scheme 1d, middle). In the DMF/DPE mixed solvent system, the PAA blocks maintained their coil-like conformation, while the outer PEO blocks collapsed owing to the favorable interactions between DMF and PAA as well as PEO and the unfavorable interactions between DPE and PEO. A well-defined structure with coil-like PAA blocks inside and collapsed PEO blocks outside was obtained and employed for the conversion of the $HAuCl_4$ precursors into the Au shell. Finally, magnetic/plasmonic Fe_3O_4/Au core/shell nanoparticles with PEO blocks intimately and permanently tethered to their surface were thus produced (Scheme 1d, right).

Transmission electron microscopy (TEM) images of three as-prepared magnetic Fe_3O_4 core nanoparticles with diameters of 6 ± 0.4, 10 ± 0.6, and 20 ± 0.5 nm, are shown in the Supporting Information, Figure S1 a–c. These particles were obtained by varying the molecular weight of the inner P4VP chain during the ATRP of 4VP. Obviously, uniform Fe_3O_4 core nanoparticles directly linked by PEO-*b*-P*t*BA were obtained. The HRTEM image of a Fe_3O_4 nanoparticle clearly shows its lattice fringe with a lattice spacing of 0.1420 nm, corresponding to the (440) plane of Fe_3O_4 crystals (Figure S1 b). The X-ray diffraction (XRD) pattern of the Fe_3O_4 nanoparticles is shown in Figure S1 d. The peaks at scattering angles of 31.3°, 36.9°, 44.8°, 54.5°, 57.8°, and 64.5° correspond to diffraction from the (220), (311), (400), (422), (511), and (440) crystal planes of Fe_3O_4 with an inverse spinel structure. All of the peaks can be indexed to Fe_3O_4 (JCPDS No. 26-1136) with a lattice parameter of 0.8090 nm.

A series of magnetic/plasmonic Fe_3O_4/Au core/shell nanoparticles with precisely tailored Fe_3O_4 core diameters and Au shell thicknesses are displayed in Figure 1. Obviously, the uniformity of the resulting core/shell nanoparticles was retained after the independent growth of a Au shell on the Fe_3O_4 core when star-like P*t*BA-*b*-PEO situated on the surface of the Fe_3O_4 core was used as a nanoreactor. The sizes of the Fe_3O_4 cores and Au shells and the corresponding volume ratios are summarized in Table S1. The size distribution for the core/shell nanoparticles was found to be less than ± 2.0 nm, suggesting that the length of the intermediate PAA blocks was well-controlled during the ATRP of *t*BA. Interestingly, when the thickness of the Au shell was larger than or comparable to the diameter of the Fe_3O_4 core, it was difficult to distinguish the core/shell morphology in a regular TEM image (i.e., not by HRTEM) because of the much higher electron density of Au than Fe_3O_4. However, for a nanoparticle with a 5 nm thick Au shell on a 20 nm Fe_3O_4 core, the core/shell structure could be seen, and the core and shell were marked with black circles (Figure 1 f). A representative HRTEM image from a 6 nm Fe_3O_4/5 nm Au core/shell nanoparticle confirmed the core/shell structure (Figure 1 b).

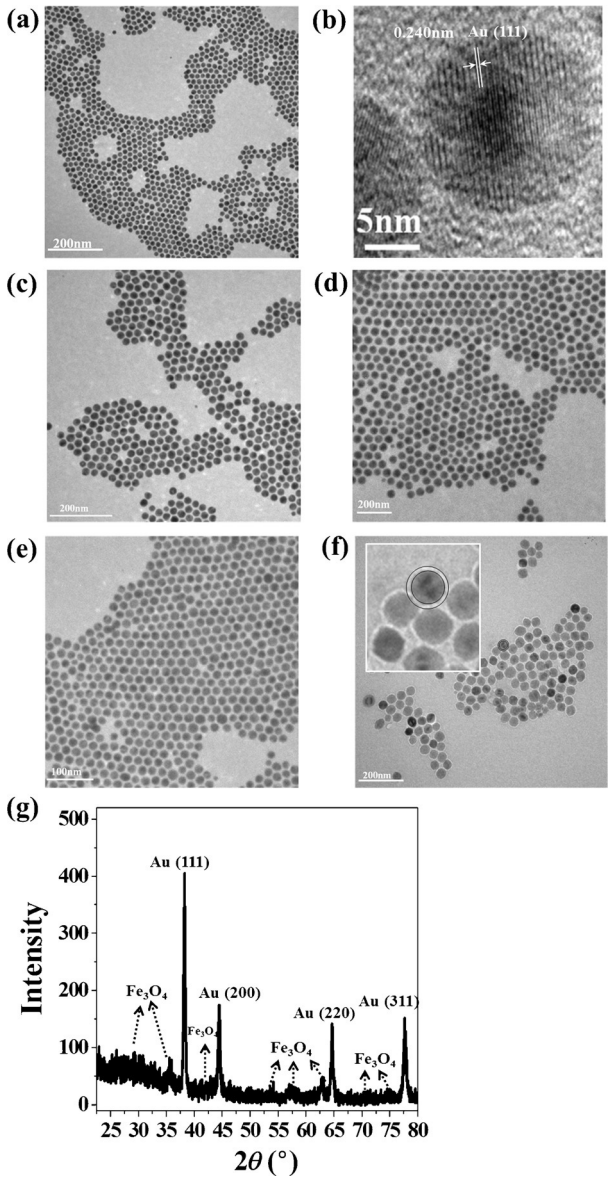

Figure 1. a, c–f) TEM images of PEO-capped Fe_3O_4/Au core/shell nanoparticles with various dimensions. The diameters of the Fe_3O_4 cores are 6 (a), 6 (c), 6 (d), 10 (e), and 20 nm (f), whereas the thicknesses of the Au shells are 5 (a), 10 (c), 18 (d), 5 (e), 5 nm (f). The black circles were added to guide the eye. The inset in (f) is a magnified image of the region marked with black circles. b) Representative HRTEM image of the core/shell nanoparticles. g) XRD pattern confirming the coexistence of Fe_3O_4 and Au in the core/shell nanoparticles.

The lattice spacing of the Au shell was found to be 0.240 nm, corresponding to the (111) plane of Au crystals. Clearly, on the basis of the HRTEM images in Figure S1 b and Figure 1 b, the Fe_3O_4 core with the [400] crystal orientation and the Au shell with the [111] crystal orientation displayed a large lattice mismatch (69 %; $\delta = \left|\left(d_{Fe_3O_4} - d_{Au}\right)/d_{Fe_3O_4}\right|$), signifying that our strategy based on a star-like triblock copolymer nanoreactor enabled the synthesis of high-quality core/shell nanoparticles while obviating the need for matching lattices between two dissimilar materials.

The XRD pattern of the Fe_3O_4/Au core/shell nanoparticles is shown in Figure 1 g. The characteristic peaks at scattering angles of 36.8°, 44.5°, and 64.8° correspond to the (111), (200), and (220) crystal planes of Au, respectively. Interestingly, the diffraction peaks from the Fe_3O_4 core were weakened by the Au coating.

HRTEM images and XRD patterns (Figure 1 b, g as well as Figure S1 b, e) showed that the Fe_3O_4 core and the Au shell possessed good crystallinity. The formation of the polycrystalline Au shell may be explained as follows. Au seeds are initially formed on the PAA chains owing to the strong coordination interactions between Au^{3+} ions derived from the $HAuCl_4{\cdot}3H_2O$ precursors and the carboxylic acid groups of PAA in star-like PAA-*b*-PEO (i.e., Fe_3O_4-PAA-*b*-PEO). Subsequently, the Au seeds evolve into nanocrystals that are encapsulated by the PAA chains. The nanocrystals on adjacent PAA chains spontaneously self-organize through an oriented attachment mechanism.[14] In this process, crystalline particles on adjacent PAA chains join each other at a planar interface and share a common crystallographic orientation. The bonding between the particles reduces the overall energy by reducing the energy penalty associated with not fully coordinated surface atoms, forming a polycrystalline Au shell. As the PAA-*b*-PEO chains situated on the surface of the Fe_3O_4 core are flexible and free (i.e., only one end is anchored on the Fe_3O_4 surface), the Au shell can grow in the way described above. To further confirm that the nanoparticles prepared by this nanoreactor approach are highly crystalline, plain Au nanoparticles were also synthesized using P*t*BA-*b*-PEO (pure P*t*BA-*b*-PEO, not Fe_3O_4-PAA-*b*-PEO; see the Experimental Section in the Supporting Information) as a nanoreactor. The corresponding HRTEM image is shown in Figure S2. The lattice fringe can be clearly seen, suggesting that the Au nanoparticles are again highly crystalline.

The absorption spectra of pure, PEO-capped Fe_3O_4 nanoparticles with different diameters (6, 10, and 20 nm) that were prepared using P*t*BA-*b*-PEO as the nanoreactor (see the Experimental Section in the Supporting Information) are compared in Figure 2 a. The absorption intensity increased as the diameter of the nanoparticle increased. The Fe_3O_4 nanoparticles exhibited a strong, yet featureless absorption in the UV/Vis range. Intervalence charge transfer has been reported to be an important contribution to absorption.[15] Aside from intervalence charge transfer, pair excitations that result from the simultaneous excitation of two neighboring, magnetically coupled Fe^{3+} ions contribute to the absorption of Fe_3O_4 nanoparticles at wavelengths of 400–600 nm.[15a] A weak band at approximately 470 nm can be attributed to Fe^{3+} ligand-field transitions.[15a] Pure PEO-capped Au nanoparticles, which served as a control, showed a strong plasmonic absorption in the visible region of the electromagnetic field at approximately 520 nm.[18b] The plasmonic absorption mainly originates form the energy coupling of the local optical field and the collective oscillation of free electrons in the Au nanoparticles. It is clear that in our study, the position of the plasmonic peak is independent of the diameter of the Au nanoparticles when the Au nanoparticles are small (i.e., < 36 nm; Figure 2 b). Absorption spectra of the Fe_3O_4/Au core/shell nanoparticles are shown in Figure 2 c. For

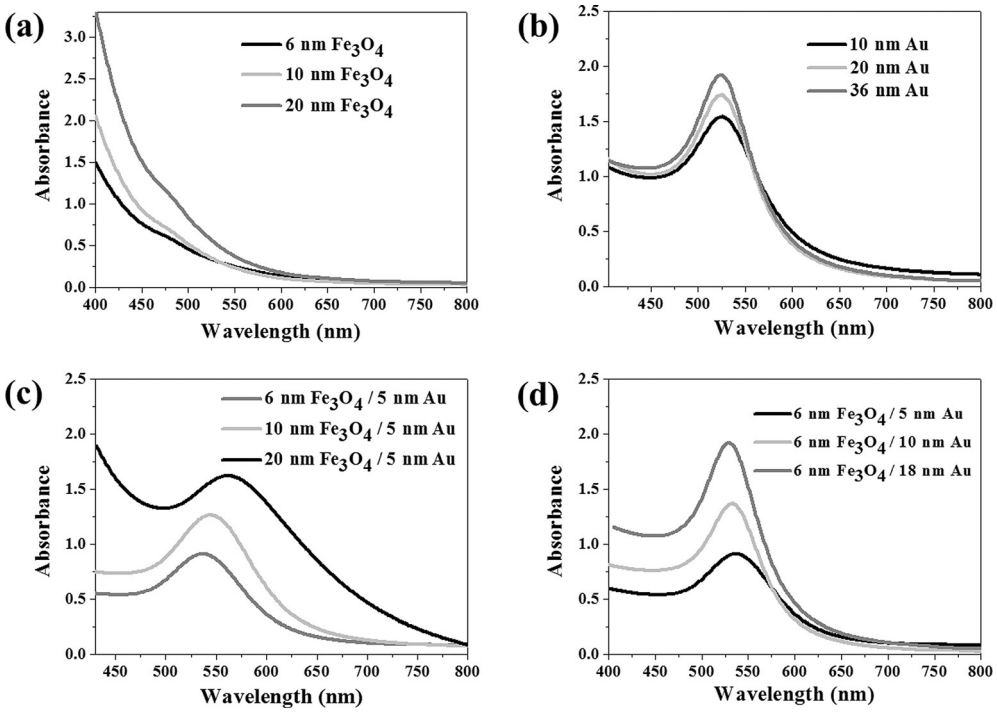

Figure 2. Visible-light absorption spectra of various nanoparticles. a) Pure Fe_3O_4 nanoparticles with diameters of 6, 10, and 20 nm. b) Pure Au nanoparticles with diameters of 10, 20, and 36 nm. c) Fe_3O_4/Au core/shell nanoparticles with Fe_3O_4 core diameters of 6, 10, and 20 nm and a fixed Au shell thickness of 5 nm. d) Fe_3O_4/Au core/shell nanoparticles with Au shell thicknesses of 5, 10, and 18 nm and a fixed Fe_3O_4 core diameter of 6 nm.

particles for which the diameters of the Fe_3O_4 cores were 6, 10, and 20 nm while the thickness of the Au shells was fixed at 5 nm, the absorption maxima were observed at 530, 540, and 563 nm, respectively.

Two typical explanations for the shift in the plasmonic peaks have been reported; these are based on the variation of the electron population on Au[16] and the plasmon modes coupling theory.[17] According to the first theory, the excess electrons in the Au shell can lead to a blue shift of the plasmonic absorption, whereas electron deficiency causes a red shift. In comparison with pure Au nanoparticles that were synthesized employing P*t*BA-*b*-PEO as a nanoreactor, the absorption maxima of the Fe_3O_4/Au core/shell nanoparticles (capitalizing on P4VP-*b*-P*t*BA-*b*-PEO as the nanoreactor) were shifted to longer wavelengths, and the magnitude of the shift increased with an increase in the Fe_3O_4 core diameter. This result indicates the absence of electrons on Au, which is in line with literature reports.[18] The electron deficiency on Au may be ascribed to the fact that the free electrons of the Au nanoparticles compensate for the charge induced by the polarized interface or that the electrons are trapped at Fe_3O_4/Au interfacial defects. According to the plasmon modes coupling theory, owing to the core/shell structure of the Fe_3O_4/Au nanoparticles, the Au shell is a two-interface system and thus possesses two distinct plasmon modes: an outer-shell surface sphere mode and an inner-shell surface cavity mode, which couple with one another, leading to the splitting into two new modes. The antisymmetric combination of these modes results in a higher-energy (blue-shifted) plasmon mode, while the symmetric combination results in a lower-energy (red-shifted) plasmon mode. The position of the plasmon resonance is thus determined by the extent of splitting. The thickness of the metallic shell represents the distance over which this interaction takes place. In this work, the absorption spectra were calculated by simulating the optical field distribution. The magnitude of the red shift increased with a decrease in the Au shell thickness, signifying that the mode coupling increased with a decrease in the interaction distance. The calculations are in good agreement with the plasmon modes coupling theory.

Furthermore, the influence of the Au shell thickness on the plasmonic absorption of the Fe_3O_4/Au core/shell nanoparticles was also scrutinized. The plasmonic absorption spectra of core/shell nanoparticles with the same Fe_3O_4 core diameter, but Au shells with various thicknesses are shown in Figure 2d. The absorption maxima at 537, 533, and 528 nm correspond to samples with Au shell thicknesses of 5, 10, and 18 nm, respectively. Interestingly, the absorption peak shifted to shorter wavelengths with an increase in the Au shell thickness. As the Au/Fe_3O_4 volume ratios were increased (Table S1), the effect of the Fe_3O_4 core diameter on the plasmonic absorption of the Au shell decreased, and the peak was blue-shifted towards its position for pure Au nanoparticles. According to the plasmon modes coupling theory,[17] the interaction distance of the two modes increases with an increase in the Au shell thickness, thereby reducing the magnitude of the red shift.

To study the effects of the diameter of the Fe_3O_4 core and the thickness of the Au shell on the optical properties of the magnetic/plasmonic core/shell nanoparticles, we then turned our attention to the simulation of the absorption cross-section of the Fe_3O_4/Au core/shell nanoparticles (Au-coated magnetic Fe_3O_4) in the range of the surface plasmon resonance absorption of Au. On the basis of TEM studies of as-prepared nanoparticles, a calculation model for nanoparticles in aqueous solution at a certain concentration was established (Figure S3a,b). The hydrophilic PEO chains together with water are assumed to form a mixed layer outside the water-soluble core/shell nanoparticles. In our calculation, this mixed layer is equivalent to a medium layer, in which the layer thickness was selected to be 1 nm, and the refractive index is

the sum of the water refractive index and a small additional component that is due to the presence of the PEO chains. We constructed a geometric model in the two-dimensional axisymmetric coordinate because of the axially symmetric structure of the nanoparticles. As the surrounding medium comprises a mixture of water and core/shell nanoparticles, we modified the dielectric function of water by introducing a parameter relevant to the concentration and dielectric constant of nanoparticles. The effective dielectric constant of the core/shell nanoparticles was calculated based on Eq. (S5) (see the Theoretical Modeling Section in Supporting Information). An example of the surface mesh discretization and the optical field distribution of Fe_3O_4/Au core/shell nanoparticles with a core diameter of 6 nm, a 5 nm thick shell, and a 1 nm mixed layer is illustrated in Figure S3c.

Although quantitative analysis of the absorption spectra of nanoparticles can be carried out by means of either discrete dipole approximation (DDA) or the finite element method (FEM),[19] the latter allows for an easy calculation of a model with arbitrary heterogeneity and a complex structure and was thus chosen for this work. The simulated absorption spectra of pure Fe_3O_4 and Au nanoparticles are shown in Figure S4. Obviously, for both the Fe_3O_4 and Au nanoparticles, the simulated absorption spectra and the trends in peak shifting with an increase in nanoparticle size are consistent with the measured spectra (Figure 2a,b). For clarity, only one representative experimentally measured spectrum was included for comparison in Figure S4.

The calculated and experimental absorption spectra of the Fe_3O_4/Au core/shell nanoparticles are compared in Figure S6. The calculated spectra were in good agreement with the measured ones and provided useful insight into the correlation between the plasmonic peak position and the dimensions of the magnetic core and plasmonic shell (Figure S6b,d). The variation of the simulated peak position as a function of the Fe_3O_4 core diameter exhibited the same trend as the experimental one (Figure S6b). The peak position changed linearly from 536 to 605 nm with an increase in the diameter of the Fe_3O_4 core from 6 to 20 nm. Moreover, the increase in the thickness of the Au shell led to a red shift of the absorption peak (Figure S6d). When the Au shell thickness was less than 6 nm, the peak position showed an obvious red shift, whereas when the thickness was more than 6 nm, the red shift gradually reached a plateau at approximately 528 nm, which corresponds to the absorption maximum of pure Au nanoparticles in our studies (Figure S4b).

In summary, we have developed a facile strategy for synthesizing high-quality magnetic/plasmonic Fe_3O_4/Au core/shell nanoparticles by judiciously exploiting amphiphilic star-like P4VP-*b*-P*t*BA-*b*-PEO triblock copolymers with well-defined molecular architectures and molecular weights as nanoreactors. These copolymers were obtained by combining two sequential atom transfer radical polymerization (ATRP) reactions with a click reaction. Despite the highly curved surface of the magnetic core nanoparticles, the magnetic core and the plasmonic shell were grown independently, thereby overcoming the lattice-matching constraint; this represents the key to our strategy. More importantly, the diameter of the magnetic Fe_3O_4 core and the thickness of the plasmonic Au shell can be precisely tuned by accurately controlling the molecular weights of P4VP and P*t*BA, respectively, during their respective ATRP reactions, thereby yielding a series of Fe_3O_4/Au core/shell nanoparticles with various Fe_3O_4 core diameters or Au shell thicknesses. The effect of the dimensions of the core/shell nanoparticles on their optical properties (i.e., plasmonic absorption) were then scrutinized by measuring their UV/Vis absorption spectra in conjunction with theoretical modeling using the finite element method. Notably, the calculated absorption spectra were in good agreement with the experimental ones in terms of the plasmonic peak positions and the changes in the peak position as a function of either the diameter of the Fe_3O_4 core or the thickness of the Au shell. In comparison with pure Au nanoparticles, the absorption peak was shifted to a longer wavelength, and this red shift became more pronounced with an increase in the diameter of the Fe_3O_4 core. Conversely, the absorption peak was blue-shifted when the thickness of the Au shell was increased. When the Au shell was thicker than 6 nm, the red shift reached a plateau, which corresponds to the absorption maximum of pure Au nanoparticles. Clearly, the optical properties of Fe_3O_4/Au core/shell nanoparticles can be readily tailored through precise control over the core diameter and shell thickness. Our strategy is robust as it can be easily extended to synthesize core/shell nanoparticles of various materials with engineered properties, obviating the need for epitaxial linkages between the core and shell materials. Such nanoparticles could find applications in electronics, optics, optoelectronics, catalysis, sensors, bioimaging, controlled drug delivery, and cancer therapy.

Acknowledgements

We gratefully acknowledge financial support from AFOSR (FA9550-13-1-0101), the NSF (ECCS-1305087), and the National Natural Science Foundation of China (61275051, 11074312, and 11374377).

Keywords: core/shell nanoparticles · gold · surface plasmon absorption · template synthesis · triblock copolymers

How to cite: *Angew. Chem. Int. Ed.* **2015**, *54*, 12091–12096
Angew. Chem. **2015**, *127*, 12259–12264

[1] a) X. C. Pang, L. Zhao, W. Han, X. K. Xin, Z. Q. Lin, *Nat. Nanotechnol.* **2013**, *8*, 426–431; b) X. Wang, D. Liu, J. Li, J. Zhen, H. Zhang, *NPG Asia Mater.* **2015**, *7*, e158; c) J. Nai, Y. Tian, X. Guan, L. Guo, *J. Am. Chem. Soc.* **2013**, *135*, 16082–16091.

[2] R. G. Chaudhuri, S. Paria, *Chem. Rev.* **2012**, *112*, 2373–2433.

[3] J. Zhang, Y. Tang, K. Lee, M. Ouyang, *Science* **2010**, *327*, 1634–1638.

[4] Y. Jang, J. Chung, S. Kim, S. W. Jun, B. H. Kim, D. W. Lee, B. M. Kim, T. Hyeon, *Phys. Chem. Chem. Phys.* **2011**, *13*, 2512–2516.

[5] G. A. Sotiriou, A. M. Hirt, P.-Y. Lozach, A. Teleki, F. Krumeich, S. E. Pratsinis, *Chem. Mater.* **2011**, *23*, 1985–1992.

[6] a) M. Colombo, S. Carregal-Romero, M. F. Casula, L. Gutierrez, M. P. Morales, I. B. Bohm, J. T. Heverhagen, D. Prosperi, W. J. Parak, *Chem. Soc. Rev.* **2012**, *41*, 4306–4334; b) R. Hao, R. Xing,

Z. Xu, Y. Hou, S. Gao, S. Sun, *Adv. Mater.* **2010**, *22*, 2729 – 2742; c) J.-H. Lee, J.-t. Jang, J.-s. Choi, S. H. Moon, S.-h. Noh, J.-w. Kim, J.-G. Kim, I.-S. Kim, K. I. Park, J. Cheon, *Nat. Nanotechnol.* **2011**, *6*, 418 – 422; d) J. Xie, G. Liu, H. S. Eden, H. Ai, X. Chen, *Acc. Chem. Res.* **2011**, *44*, 883 – 892.

[7] X. Zhou, W. Xu, Y. Wang, Q. Kuang, Y. Shi, L. Zhong, Q. Zhang, *J. Phys. Chem. C* **2010**, *114*, 19607 – 19613.

[8] a) K. M. Mayer, J. H. Hafner, *Chem. Rev.* **2011**, *111*, 3828 – 3857; b) K. L. Wustholz, A.-I. Henry, J. M. McMahon, R. G. Freeman, N. Valley, M. E. Piotti, M. J. Natan, G. C. Schatz, R. P. V. Duyne, *J. Am. Chem. Soc.* **2010**, *132*, 10903 – 10910.

[9] S. Pal, M. Morales, P. Mukherjee, H. Srikanth, *J. Appl. Phys.* **2009**, *105*, 07B504.

[10] a) H.-M. Song, Q. Wei, Q. K. Ong, A. Wei, *ACS Nano* **2010**, *4*, 5163 – 5173; b) Y. Zhai, J. Zhai, Y. Wang, S. Guo, W. Ren, S. Dong, *J. Phys. Chem. C* **2009**, *113*, 7009 – 7014.

[11] H. Zhu, E. Zhu, G. Ou, L. Gao, J. Chen, *Nanoscale Res. Lett.* **2010**, *5*, 1755 – 1761.

[12] C. S. Levin, C. Hofmann, T. A. Ali, A. T. Kelly, E. Morosan, P. Nordlander, K. H. Whitmire, N. J. Halas, *ACS Nano* **2009**, *3*, 1379 – 1388.

[13] a) A. Roldan, D. Santos-Carballal, N. H. de Leeuw, *J. Chem. Phys.* **2013**, *138*, 204712; b) A. Januszko, S. K. Bose, *J. Phys. Chem. Solids* **2015**, *82*, 67 – 75.

[14] R. L. Penn, J. F. Banfield, *Science* **1998**, *281*, 969 – 971.

[15] a) Y. P. He, Y. M. Miao, C. R. Li, S. Q. Wang, L. Cao, S. S. Xie, G. Z. Yang, B. S. Zou, C. Burda, *Phys. Rev. B* **2005**, *71*, 125411; b) W. F. J. Fontijn, P. J. van der Zaag, L. F. Feiner, R. Metselaar, M. A. C. Devillers, *J. Appl. Phys.* **1999**, *85*, 5100 – 5105.

[16] M.-C. Daniel, D. Astruc, *Chem. Rev.* **2004**, *104*, 293 – 346.

[17] P. K. Jain, M. A. El-Sayed, *Nano Lett.* **2007**, *7*, 2854 – 2858.

[18] a) Y. Sheng, J. Xue, *J. Colloid Interface Sci.* **2012**, *374*, 96 – 101; b) H. Yu, M. Chen, P. M. Rice, S. X. Wang, R. L. White, S. Sun, *Nano Lett.* **2005**, *5*, 379 – 382.

[19] a) O. L. Muskens, G. Bachelier, N. D. Fatti, F. Vallée, A. Brioude, X. Jiang, M.-P. Pileni, *J. Phys. Chem. C* **2008**, *112*, 8917 – 8921; b) Y. R. Davletshin, A. Lombardi, M. F. Cardinal, V. Juvé, A. Crut, P. Maioli, L. M. Liz-Marzán, F. Vallée, N. D. Fatti, J. C. Kumaradas, *ACS Nano* **2012**, *6*, 8183 – 8193.

Received: May 23, 2015
Revised: July 10, 2015
Published online: August 31, 2015

